A model of oxygen dynamics in the cerebral microvasculature and the effects of morphology on flow and metabolism

Chang Sub PARK [*], Stephen J. PAYNE

* Corresponding author: Tel.: ++44 (0)1865 617696; Fax: ++44 (0)1865 617703; Email:
chang.park@eng.ox.ac.uk
Institute of Biomedical Engineering, Department of Engineering Science, University of Oxford, Oxford, UK

Abstract The cerebral microvasculature plays a vital role in adequately supplying blood to the brain. Determining the health of the cerebral microvasculature is important during pathological conditions, such as stroke and dementia. Recent studies have shown the complex behaviour of cerebral metabolic rate with transit time distribution. In this paper, we extend a recently developed technique to solve for residue function and transit time distribution in an existing physiologically accurate model of the cerebral microvasculature to calculate cerebral metabolism. We present the mathematical theory based on solving the mass transport equation followed by results of the simulations. It is found that oxygen extraction fraction and cerebral metabolic rate are dependent on both mean and heterogeneity of the transit time distribution. For changes in cerebral blood flow, a positive correlation can be observed between mean transit time and oxygen extraction fraction, and a negative correlation between mean transit time and metabolic rate of oxygen. The metabolic rate is thus affected more significantly by cerebral blood flow than oxygen extraction fraction. A negative correlation can also be observed between transit time heterogeneity and the metabolic rate of oxygen for a constant cerebral blood flow. The heterogeneity of the transit time distribution also has an effect on the response of oxygen extraction fraction and cerebral metabolic rate to sudden changes. These results provide information on the role of the cerebral microvasculature and its effects on flow and metabolism. They thus open up the possibility of obtaining additional valuable clinical information for diagnosing and treating cerebrovascular diseases.

Keywords: Microcirculation, Oxygen Dynamics, Oxygen Extraction Fraction, Cerebral Metabolic Rate

1. Introduction

Measurements of cerebral blood flow (CBF), mean transit time (MTT), oxygen extraction fraction (OEF) and cerebral metabolic rate of oxygen ($CMRO_2$) have been widely used in clinical studies to diagnose ischaemic lesions, where CBF is the flow of blood per volume of tissue, MTT is the ratio of the cerebral blood volume (CBV) to CBF, with CBV being the volume of blood per volume of tissue, OEF is the ratio of oxygen removed to oxygen supplied and $CMRO_2$ is the product of CBF and the oxygen removed. Studies using positron emission tomography have shown regions of brain tissue surviving during ischaemia. The tissue is characterised by a reduction in CBF and an increase in oxygen extraction to meet the necessary metabolic demand (Baron *et al*., 1981, Powers *et al*., 1987). Detecting such tissues is clinically important, especially in ischaemic stroke, as it helps to determine the tissue at risk.

CBF has been thought to be tightly coupled to the metabolic needs of tissue. Models of oxygen delivery have attempted to provide a better understanding of the coupling between CBF and $CMRO_2$. Buxton and Frank (1997) considered a model of oxygen transport from the capillary to the tissue to predict a high coupling ratio due to physiological limitations of oxygen delivery. The model assumed steady state oxygen concentration, constant oxygen permeability and ratio of plasma to blood oxygen concentration, and negligible tissue

oxygen concentration. Hyder *et al*., (1998) introduced dynamic changes in oxygen permeability to provide a better fit to *in vivo* data of changes in CBF and $CMRO_2$. Hayashi *et al*., (2003) considered varying oxygen diffusivity and nonlinear binding of haemoglobin to oxygen. Zheng *et al*., (2002) included dynamic changes in oxygen transport as well as relaxing the assumption of negligible tissue oxygen concentration.

More recently, there has been an interest in the heterogeneity of the flow patterns and the effects of the transit time distribution. Jespersen and Østergaard (2012) considered a non-physiological network of parallel equal length capillary vessels with an underlying transit time distribution to determine the available oxygen concentration and its effects with changes in transit time distribution. The results show that, even for a simple network, a complex nonlinear behaviour in OEF and $CMRO_2$ with both individual and combinational changes in mean and variance of the transit time distribution can be observed. However, given the inter-connectedness of the capillary network and studies suggesting flow distribution and thus transit time distribution being significantly dependent on network morphology (Pries *et al*., 1996) and network density (Park and Payne, 2013), any *in vivo* comparison will require models with physiologically accurate microvascular networks.

Generating physiologically accurate microvascular networks is extremely difficult due to the inter-connectedness of the capillary network. Artificial microvascular networks have thus been generated using specific algorithms (Linniger *et al*., 2013, Su *et al*., 2012). Linninger *et al*., (2013) applied this to understand oxygen exchange between blood vessels and brain cells by quantifying oxygen advection in the microcirculation, tissue oxygen perfusion and oxygen consumption. Su *et al*., (2012) considered the effects of the morphological properties on the transport of blood.

These studies both suggested that the morphology of the cerebral microvasculature appears to play an important role in the adequate supply of oxygen to the cerebral tissue, which will have an important role during ischaemia. In this paper we thus developed a dynamic oxygen transport model in physiologically accurate artificial capillary networks, previously developed by Su *et al*., (2012), to quantify the relationship between MTT, mean absolute deviation transit time (MADTT), OEF and $CMRO_2$ with varying morphological properties. This approach enables us to extract further information about the microvasculature, which may have potential clinical value for diagnosis and treatment.

2. Theory

General capillary networks are generated to solve for oxygen transport. A minimum spanning tree algorithm is used to randomly generate physiologically accurate capillary networks (Su *et al*., 2012) based on the matching of histological data from experiments (Cassot *et al*., 2006). Su *et al*., (2012) solve for the flow assuming Poiseuille flow with individual vessel viscosity obtained from an experimental relationship (Pries *et al*., 1992) by applying a pressure gradient and taking the net flow at the nodes to be zero. Once the flow distribution is determined, oxygen concentration in the capillary network can be obtained by solving the mass transport equation. The approach considered here is an extension to that proposed by Park and Payne (2013) to solve for the residue function in microvascular networks assuming that the concentration is driven solely by convection, with the extension proposed here being the addition of a tissue diffusion term with a rate proportional to the difference in oxygen concentration between the plasma and the tissue. Assuming that oxygen in the tissue is consumed rapidly such that tissue oxygen concentration is negligible, and that the fraction of oxygen concentration in plasma to blood is constant, the one-dimensional mass transport for a single vessel can be expressed

as:

$$\frac{\partial C(x,t)}{\partial t} + U\frac{\partial C(x,t)}{\partial x} = -\lambda C(x,t), \qquad (1)$$

where C is the oxygen concentration, x is the axial coordinate, t is time, U is the velocity and λ is the product of the surface permeability and the fraction of oxygen concentration in the plasma to blood. Considering the Laplace transform of equation (1) with $C(x,t=0)=0$, the oxygen concentration can be expressed in the s-domain as:

$$C(x,s) = C(0,s)\exp\left[-\frac{(s+\lambda)x}{U}\right]. \qquad (2)$$

The oxygen concentration at the outlet in the time-domain, for a given inlet concentration, can be obtained by taking the inverse Laplace transform of equation (2). Considering a unit step function, $u(t)$, for simplicity, with a magnitude of A at the vessel inlet, such that $C(0,s)=A/s$, the outlet concentration can be expressed in time-domain as:

$$C(L,t) = Au(t-T)e^{-\lambda T}, \qquad (3)$$

where L is the length of the vessel and $T=L/U$ is the transit time. Since the concentration is convection driven, the outlet concentration is a simple step function with a delay T. The magnitude of the concentration then depends on the amount of oxygen diffused into the tissue.

For a capillary network, it is necessary to consider the distribution of oxygen concentration at the nodes where the vessel junctions occur. The concentration at each node is taken to be the sum of all supplying vessels weighted with the flow rates:

$$C_j(s) = \frac{\sum_i C_{ij}(L_{ij},s)Q_{ij}}{\sum_i Q_{ij}}, \qquad (4)$$

where Q represents flow rate. The subscripts represent the nodes being considered; j represents node j whilst ij represents from node i to node j. Note that nodes i and j are only considered if these are connected as the parameters will be equal to zero when the nodes are not connected. From equation (4), the outlet concentration of the network can be expressed in the s-domain as:
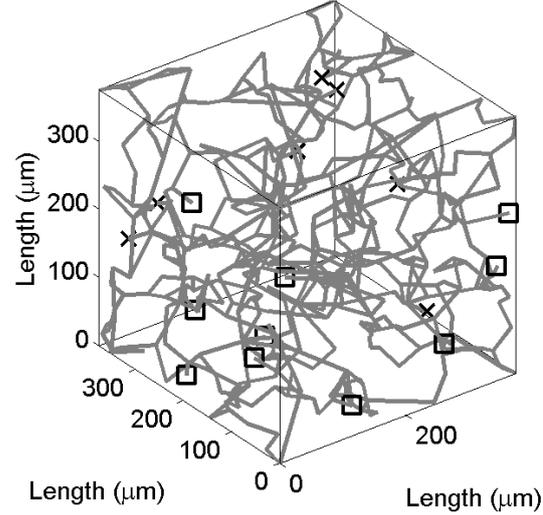

Fig. 1. A sample capillary network. The square and cross markers represent the inlets and outlets respectively.

$$C_v(s) = \frac{C_a(s)}{Q_{net}}\sum_{i,v}\prod_{m,n}^{i}Q_{iv}e^{-(s+\lambda_{iv})T_{iv}}$$
$$\times \frac{Q_{mn}}{\sum_a Q_{an}}e^{-(s+\lambda_{mn})T_{mn}}, \qquad (5)$$

where subscripts a and v are the network inlet and outlet nodes respectively, and Q_{net} is the net flow in the capillary network. Note that only four parameters are required to determine the concentration, these being L, R, U and λ. L, R and λ are solely properties of the network whilst U is also dependent on the pressure difference, Δp, applied.

Taking the inverse Laplace transform of equation (5) with a given inlet concentration function, it is possible to obtain the outlet concentration in the time-domain. OEF can then be obtained from:

$$OEF(t) = \frac{C_a(t) - C_v(t)}{C_a(t)}, \qquad (6)$$

and CMRO$_2$ can be obtained from:

$$CMRO_2(t) = CBF \cdot C_a(t) \cdot OEF(t). \qquad (7)$$

3. Results and Discussion

Two different sized network cubes are considered here each with an inlet and outlet density matching that obtained from experimental results (Cassot et al., 2010). Fig.

1 shows a sample capillary network generated with matching morphological properties. A step change in the concentration at the inlet is considered:

$$C_a(t) = \alpha[1 + \beta u(t - \tau)] \qquad (8)$$

where α is the magnitude of the concentration at the inlet, β is the percentage change in the magnitude and τ is the time at which the step change is considered. The concentration at the outlet can be obtained by taking the Laplace transform of equation (8), substituting this term into equation (5) and taking the inverse Laplace transform. Substituting this term and equation (8) into equation (6), OEF can be expressed as:

$$
\begin{aligned}
OEF(t) = 1 &- \frac{1}{\alpha[1 + \beta u(t - \tau)]Q_T} \\
&\times \sum_{i,v} Q_{iv} e^{-\lambda T_{iv}} \prod_{m,n}^{i} \frac{Q_{mn}}{\sum_a Q_{an}} e^{-\lambda T_{mn}} \\
&\times \left[\alpha u\left(t - \sum_{m,n}^{i} T_{mn} - T_{iv} \right) \right. \\
&\left. + \beta u\left(t - \sum_{m,n}^{i} T_{mn} - T_{iv} - \tau \right) \right].
\end{aligned}
\qquad (9)
$$

Table 1 shows the cube size and the initial conditions driving the flow and concentration between the inlets and outlets. CBF was set to 55 ml/100ml/min and λ was chosen so that OEF would be around baseline OEF of 0.4. For each cube size, 100 different networks with equivalent conditions were randomly generated to allow statistical analysis. A constant inlet concentration was first considered ($\beta = 0$) followed by a step decrease in the magnitude of the inlet concentration ($\beta = -0.2$).

Table 1
Initial conditions for the networks considered.

	Edge length (μm)	
	250	375
Inlet:outlet	3:2	10:7
α (μmol/ml)	9	
β	0, -0.2	
λ	0.3	

Table 2 shows the steady state mean and standard deviation of CBV, MTT, MADTT, OEF and $CMRO_2$ of the two cube sizes considered for a constant inlet concentration. Note that the standard deviation in each of the values obtained is larger for the smaller cube. This is probably due to a greater degree of heterogeneity in the morphological properties of the created networks at the smaller length scale. MTT and MADTT can be calculated from the transit time distributions, which are obtained according to the method proposed by Park and Payne (2013). MADTT is considered here instead of the more typical standard deviation as the transit time distribution is heavily skewed positively with a long tail making the standard deviation prone to outliers.

Table 2
Mean and standard deviation of CBV, MTT, MADTT, OEF and $CMRO_2$ for the two cube sizes.

	Edge length (μm)	
	250	375
CBV (%)	1.46±0.09	1.46±0.04
MTT (s)	1.59±0.10	1.59±0.04
MADTT (s)	1.26±0.32	1.24±0.18
OEF	0.41±0.05	0.42±0.03
$CMRO_2$ (μmol/ml/min)	1.64±0.20	1.67±0.12

There is no significant difference between the mean values in CBV, MTT, MADTT, OEF and $CMRO_2$ of the two cube sizes as expected since these are determined by the morphological properties, which were matched for both cube sizes. Although MTT is similar for both cube samples, a smaller MADTT is observed for the larger cube, mainly due to the decrease in the heterogeneity of the morphological properties, which leads to a larger OEF. This observation is in agreement with the result obtained by Jespersen and Østergaard (2012) with their non-physiological network of parallel equal length capillary vessels where, for a constant MTT, OEF increased with decreasing variance of the transit time. This is due to the overall magnitude of the concentration at the outlet depending on the sum of all the individual pathway transit times as well as MTT. Since
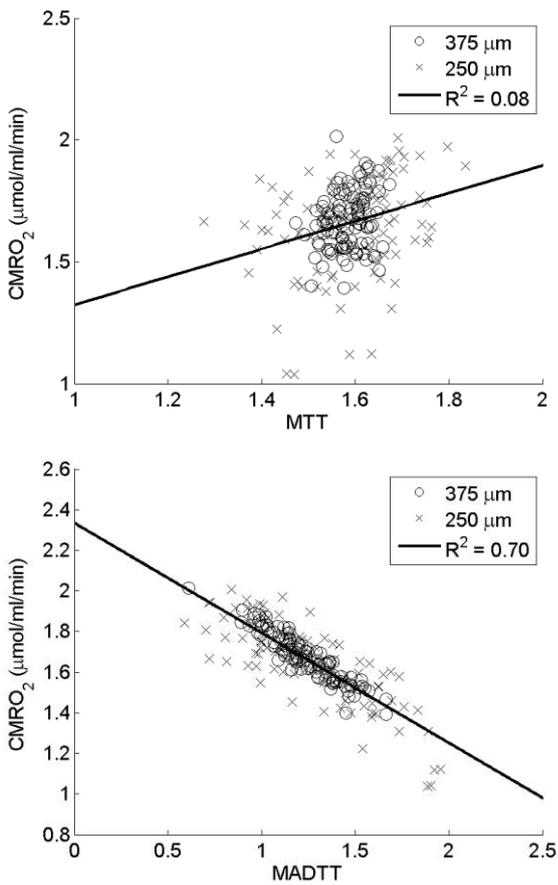
Fig. 2 Plot of MTT and MADTT against $CMRO_2$ for a constant CBF.

Fig. 3 Plot of MTT against OEF and $CMRO_2$ for varying CBF.

the larger cube has a smaller mean MADTT, mean OEF and mean $CMRO_2$ are larger. Fig. 2 shows the variation of $CMRO_2$ with MTT and MADTT. A linear regression is considered here to quantify the correlation between the parameters due to the simplicity in the analysis and by no means establishes that the two parameters have a linear relationship. Since CBF is kept constant, the plot of OEF will only differ with the plot of $CMRO_2$ in magnitude and thus it is not shown here. No clear trend can be observed between MTT and $CMRO_2$ (R^2=0.08) due to the small difference in MTT between the different networks. There is however, a negative correlation between $CMRO_2$ and MADTT (R^2=0.70) agreeing with the above observation that the transit time distribution heterogeneity also affects OEF and $CMRO_2$.
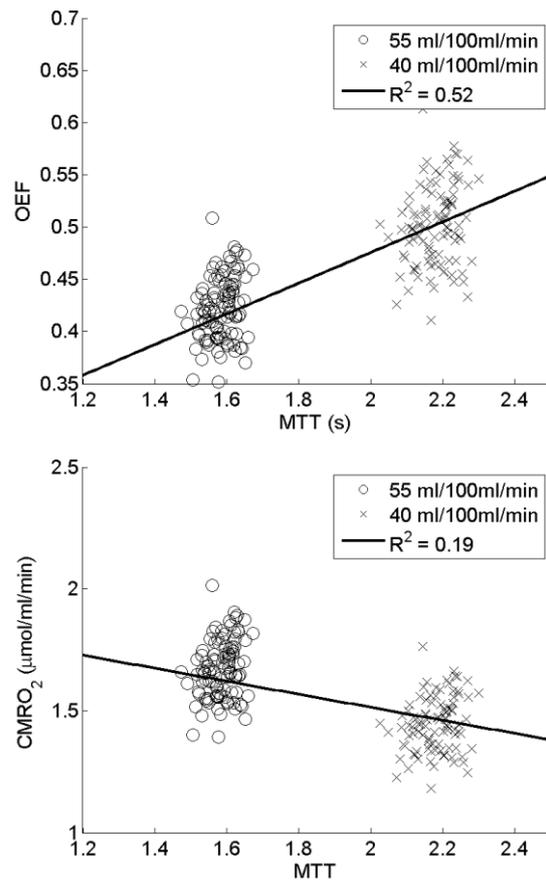
A change in CBF was next considered to

determine the effects of changes in MTT. Fig. 3 shows the variation of MTT with OEF and $CMRO_2$ respectively for the larger cube. Once more, a linear regression is considered to quantify the correlation between the parameters. A positive correlation can be observed between MTT and OEF (R^2=0.52). As MTT increases as a result of a decrease in CBF, OEF will increase as there is more time for oxygen to be extracted to maintain $CMRO_2$. However, OEF increase is constrained by the amount of oxygen available. Thus $CMRO_2$ will eventually drop as CBF decreases. There will be a further drop with increasing MADTT as MADTT increase also leads to a decrease in OEF. Jespersen and Østergaard (2012) showed that $CMRO_2$ could increase or decrease with heterogeneity of the flow for a constant MTT. These results suggest that MTT is more dependent on the initial conditions than the morphological properties whilst MADTT is dependent on both.
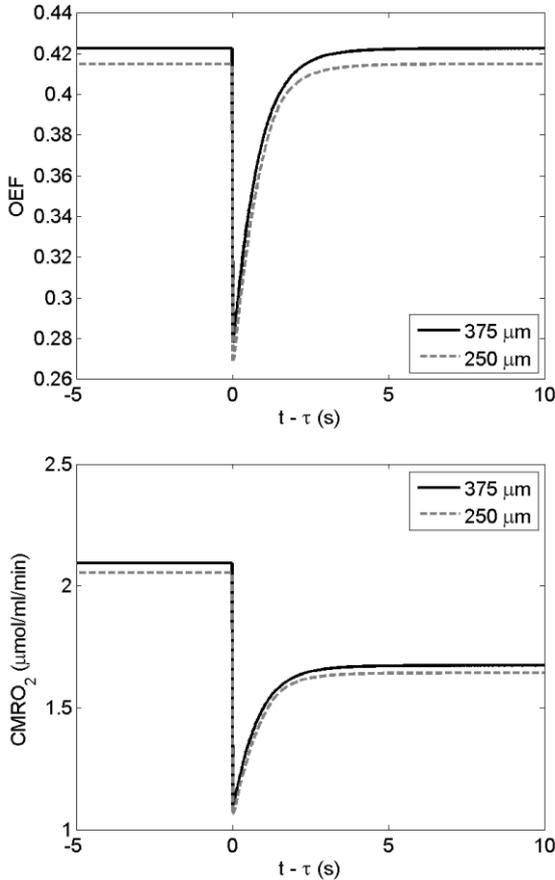
Fig. 4. Mean OEF and CMRO$_2$ for dynamic changes in the concentration at the inlet.

In order to observe the response of the network for a dynamic change, a step decrease function in the inlet concentration is considered at $t=\tau$. Fig. 4 shows the effects of the step change in mean OEF and CMRO$_2$. For each cube size, a sharp decrease in both mean OEF and mean CMRO$_2$ is observed initially, gradually returning back to its original steady state value for mean OEF and to 80% for mean CMRO$_2$ due to the drop of the inlet concentration by 20%. The time for this recovery to occur for both cubes is around 5s. An exponential recovery curve fitted to each plot shows the time constant for both the larger and smaller cubes to be 0.84s. Thus cube size does not have an effect on the recovery.

The ultimate aim of this work is for clinical applications in pathological conditions such as ischaemic stroke. This will require comparing the results obtained with clinical results.

Although the preliminary results show that cube size does not affect the solution, any direct comparison with clinical data will still require matching it to image voxel sizes as the cubes considered here do not consider vessels linking from neighbouring cubes. Scaling up the cubes generated here will require a different approach, for example, the multi-scale approach proposed by Shipley and Chapman (2010). This will be the subject of future work. It should be noted that the assumption that λ is constant across the network was considered here due to the significant variability between the studies. Also, negligible tissue oxygen concentration was considered for simplicity of the analysis. In each case the assumption can easily be relaxed to increase the complexity of the model at a relatively low computational cost.

4. Conclusion

An extension to a recently developed mathematical technique to solve for the residue function in a capillary network with matching physiological topology has been developed here to solve for OEF and CMRO$_2$. The results show that the size of the tissue considered does not affect the solution as long as the morphological properties in both cases are matched. However, great care needs to be taken when directly comparing biomarkers obtained here with clinical data as the artificial cube considered here does not have vessels linked to neighbouring cubes. The simulations show that OEF correlates with both MTT and MADTT whilst CMRO$_2$ correlates with MADTT suggesting the importance of both parameters defining the transit time distribution. For the dynamic case, a step change in the concentration at the inlet leads to a sharp change in OEF followed by a gradual recovery. Once again, this recovery is dependent on the properties of the transit time distribution.

Acknowledgements

Reference

Baron, J.C., Bousser, M.G., Rey, A., Guillard, A., Comar, D., Castaigne, P., 1981. Reversal of focal "misery-perfusion syndrome" by extra-intracranial arterial bypass in hemodynamic cerebral ischemia. A case study with ^{15}O positron emission tomography. Stroke 12, 454–459.

Buxton, R.B., Lawrence, R.F., 1997. A model for the coupling between cerebral blood flow and oxygen metabolism during neural stimulation. J. Cereb. Blood Flow Metab. 17, 64-72.

Cassot, F., Lauwers, F., Fouard, C., Prohaska, S., Lauwers-Cances, V., 2006. A novel three-dimensional computer-assisted method for a quantitative study of microvascular networks of the human cerebral cortex. Microcirculation 13, 1-18.

Cassot, F., Lauwers, F., Lorthois, S., Puwanarajah, P., Cances-Lauwers, V., Duvernoy, H., 2010. Branching patterns for arterioles and venules of the human cerebral cortex. Brain Res. 1313, 62-78.

Hayashi, T., Watabe, H., Kudomi, N., Kimi, K.M., Enmi, J.-I., Hayashida, K., Iida, H., 2003. A theoretical model of oxygen delivery and metabolism for physiologic interpretation of quantitative cerebral blood flow and metabolic rate of oxygen. J. Cereb. Blood Flow Metab. 23, 1314-1323.

Hyder, F., Shulman, R.G., Rothman, D.L., 1998. A model for the regulation of cerebral oxygen delivery. J. Appl. Physiol. 85, 554-564.

Jespersen, S.N., Østergaard, L., 2012. The roles of cerebral blood flow, capillary transit time heterogeneity, and oxygen tension in brain oxygenation and metabolism. J. Cereb. Blood Flow Metab. 32, 264-277.

Linninger, A.A., Gould, G., Marinnan, T., Hsu, C.-Y., Chojecki, M., Alaraj, A., 2013. Cerebral microcirculation and oxygen tension in the human secondary cortex. An. Biomed. Eng. 41(11), 2264-2284.

Park, C.S., Payne, S.J., 2013. A generalized mathematical framework for estimating the residue function for arbitrary vascular networks. Interface Focus 3, 20120078.

Powers, W.J., Press, G.A., Grubb, R.L.Jr., Gado, M., Raichle, M.E., 1987. The effect of hemodynamically significant carotid artery disease on the hemodynamic status of the cerebral circulation. Ann. Intern. Med. 106, 27–34.

Pries, A.R., Neuhaus, D., Gaehtgens, P., 1992. Blood viscosity in tube flow: dependence on diameter and hematocrit. Am. J. Physiol. Heart Circ. Physiol. 263, H1770-H1778.

Pries, A.R., Secomb, T.W., Gaehtgens, P., 1996. Relationship between structural and hemodynamic heterogeneity in microvascular networks. Am. J. Physiol. 270, H545–H553.

Shipley, R.J., Chapman, S.J., 2010. Multiscale modelling of fluid and drug transport in vascular tumours. Bull. Math. Biol. 72, 1464-1491.

Su, S.-W., Catherall, M., Payne, S., 2012. The influence of network structure on the transport of blood in the human cerebral microvasculature. Microcirculation 19, 175-187.

Zheng, Y., Martindale, J., Johnston, D., Jones, M., Berwick, J., Mayhew, J., 2002. A model of the hemodynamic response and oxygen delivery to brain. NeuroImage 16, 617-637.